MATERIALS SCIENCE

Phase-dependent redox insulation in mussel adhesion

Eric Valois[1]*, Razieh Mirshafian[2]*, J. Herbert Waite[1,2]†

Catecholic 3,4-dihydroxyphenyl-L-alanine (Dopa) residues in mussel foot proteins (mfps) contribute critically to mussel (*Mytilus californianus*) plaque adhesion, but only if protected from oxidation at the adhesive-substratum interface. Dopa oxidation is thermodynamically favorable in seawater yet barely detectable in plaques; therefore, we investigated how plaques insulate Dopa-containing mfps against oxidation. Seawater sulfate triggers an mfp3 and mfp6 liquid-liquid phase separation (LLPS). By combining plaque cyclic voltammetry with electrophoresis, mass spectrometry, and redox-exchange chemistry, we show that Dopa-containing mfp3 and mfp6 in phase-separated droplets remain stable despite rapid oxidation in the surrounding equilibrium solution. The results suggest that a cohort of oxidation-prone proteins is endowed with phase-dependent redox stability. Moreover, in forming LLPS compartments, Dopa proteins become reservoirs of chemical energy.

INTRODUCTION

Liquid-liquid phase changes in biomacromolecular assemblages are not confined to living cells where they facilitate dynamic compartmentalization associated with time- and location-specific reactions (*1*). A common extracellular and extra-organismic liquid-liquid phase change known as coacervation is involved in the formation of biomolecular materials as diverse as arteries (*2*), silks (*3*), beaks (*4*), butterfly wings (*5*), and marine adhesives (*6,7*). The formation of adhesive plaques by mussels (*Mytilus californianus*) involves a cohort of mostly disordered proteins known as mussel foot proteins (mfps) (*8*). Several *mfps* exhibit liquid-liquid phase separation (LLPS) (*7, 9–11*) triggered by specific chemical cues in the ambient seawater. Adaptive advantages of coacervation include fluid adhesive protein concentrates, shear thinning to facilitate fluid transport, and low interfacial energy for spontaneous spreading underwater (*4, 9, 12, 13*).

An iconic chemical feature of all *mfps* is 3,4-dihydroxyphenyl-L-alanine (Dopa), a catecholic amino acid that is post- or cotranslationally introduced into the proteins before deposition onto target surfaces. Dopa contributes appreciably to wet adhesion but only when redox poise is locally controlled. Under reducing conditions (Fig. 1A), Dopa-containing proteins dehydrate surfaces, form stable π-cation interactions and bidentate H-bonds, coordinate with metal ions and metal oxide surfaces and, in synergy with lysine, evict adsorbed salts from rock surfaces (*14, 15*). Under oxidizing conditions, Dopa becomes a quinone with strong cross-linking tendencies, but metal oxide/mineral surface binding and metal ion complexation are notably diminished (Fig. 1A) (*15*). Known interim adaptations to reduce oxidative losses, including electron-withdrawing effects on the catechol moiety (*16*), surface deposition of mfps at acidic pH (*17, 18*), and cosecretion of mfps with antioxidants (*18, 19*), are effective in temporarily optimizing adhesion under experimental conditions but do not reveal how the long-term interfacial redox poise of plaques is maintained in highly oxidizing natural seawater (*20*). In situ probes indicate that the acidic pH of nascent plaques only lasts a few minutes before equilibrating to seawater pH 8 (*17*), and yet, adhesive interfaces between plaques and substrata remain reducing for months in seawater (*21*).

Using Dopa as an intrinsic redox reporter, we investigated which proteins undergo phase separation in mature plaques and how the phase affects Dopa redox. Given reports of LLPS in organelle formation and pathogenesis in cells (*1, 22*), the importance of phase-specific redox is likely to extend beyond mussel adhesion.

RESULTS

Plaque ultrastructure

Mussel adhesive plaques (Fig. 1B) consist of an open porous architecture with two length scales of porosity (*23*). These pores appear empty by scanning electron microscopy (SEM) (Fig. 1C) but are fluid-filled in native plaques. The interfacial film is ~15 nm thick, overlaid by a continuous mottled layer ~50 to 100 nm thick before the regular ~100-nm porosity begins (Fig. 1D). Figure 1 (D and E) compares two interfaces from naturally deposited plaques. One was untreated before routine processing, whereas the other was equilibrated at pH 3 for 30 min. Although both plaques appeared identical to the eye, much interfacial plaque structure was disrupted at pH 3 vis-à-vis controls (Fig. 1E). The electron-dense film and much adjoining internal structure were dissolved, leaving a 10- to 20-nm porosity mesh. Perhaps this is evidence of pH-dependent phase transitions.

Interfacial electrochemistry

By subjecting plaque interfaces to cyclic voltammetry (CV) at pH 8 and pH 3, we observed a shift of +290 mV in the anodic potentials (E_{anode}) (Fig. 2A). The relationship between redox potential and pH is linear and characteristic of the two-electron oxidation of catechols, including Dopa (*24*) (fig. S1A) and Dopa-containing mfp3 variants (fig. S1B). The oxidation potential peak current at pH 3 is time dependent and thus is consistent with a condensed matter-to-solution phase change in the plaque (fig. S1C). The typically broader anodic peak may reflect the different local environments of Dopa in mfps (*25*). Separate analysis of plaque interfaces by x-ray photoelectron spectroscopy (XPS) also detected thiols and sulfate anions (Fig. 2B).

Electrophoretic transfer of plaque proteins

To capture and identify proteins involved in pH-induced phase transitions, we electroblotted plaques to membrane supports at different pHs (Fig. 2C). Soluble proteins showed electrokinetic migration through the porous plaque mesh under an electric field. Typically, other protein phases, e.g., coacervates, hydrogels, and precipitates,

[1]Biomolecular Science and Engineering Program, University of California, Santa Barbara, Santa Barbara, CA 93106, USA. [2]Marine Science Institute, University of California, Santa Barbara, Santa Barbara, CA 93106, USA.
*These authors contributed equally to this work.
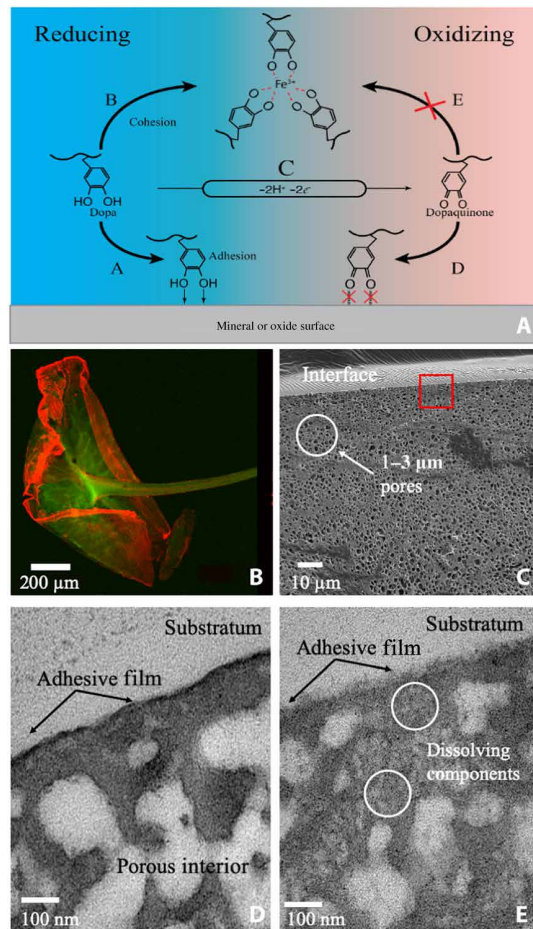†Corresponding author. Email: hwaite@ucsb.edu

Fig. 1. Plaque chemistry and architecture. (**A**) Dopa-containing mfps (spirals) recruited for adhesion by chemisorption (i) and cohesion by tris-catecholato Fe^{3+} complexation (ii). Dopa oxidized by O_2 (iii) becomes dopaquinone, which forms covalent adducts but shows reduced surface binding (iv) and coordination (v). (**B**) Plaque with intrinsic fluorescence. (**C**) SEM of plaque section; (**D**) transmission electron microscopy of untreated plaque interface; (**E**) 5% acetic acid–treated (30 min) interface.

Fig. 2. Chemical analysis of plaque interfaces. (**A**) CV plaque, pH 3 (5% acetic acid), and pH 8 (seawater) showing anodic peak potentials. Glassy carbon electrode at 50 mV/s scan rate. (**B**) XPS of plaque footprint on glass with sulfur speciation as thiol and sulfate peaks. a.u., arbitrary units. (**C**) Electroblotting strategy used to move soluble proteins: Plaque is positioned with adhesive interface facing a nitrocellulose membrane and the cathode. Nitrocellulose membrane was soaked in matrix, dried, and subjected to mass spectrometry. (**D**) Mass spectrum of electrokinetic proteins at pH 8 (red, tris glycinate) and pH 3 (black, acetic acid). Inset extends m/z range to 13,000. (**E**) Enlarged m/z of mfp3-1β showing mass register with mfp3-1β standard (purple).

stay put. Migrating proteins were electroblotted from plaques to nitrocellulose and identified by mass spectrometry and the byssal proteome of *M. californianus* (table S1A) (*8*). At pH 3, mfp3 and mfp6 variants predominated, particularly mfp3-1β [mass/charge ratio (m/z) 5192] and mfp3S (m/z 6412) variants, distinguished by the 16-Da sawtooth steps associated with Dopa modifications (Fig. 2D and table S1B). In contrast, at pH 8, m/z values consistent with mfp8 and unmodified mfp3 variants were evident; mfp6 was absent. Unmodified mfp5 was sparingly detectable (m/z 8910 Da) at pH 8, whereas fully hydroxylated (m/z 9230) mfp5 was soluble at both pHs (table S2). These results suggest that different phases of proteins coexist in the plaque under the pH 8 and salinity regimes of natural seawater. Mfp3 and mfp6 variants with Dopa are insoluble at pH 8 but can be easily rendered soluble at pH 3. Curiously, mfp3 variants without Dopa are soluble at pH 8 as is mfp8. With regard to mfp3 partitioning between solution and condensed phase, studies of hydroxylated and nonhydroxylated recombinant forms indicate that both are capable of LLPS, but the phase boundaries are different and separated by up to 2 pH units (*10*), suggesting that variants of modification
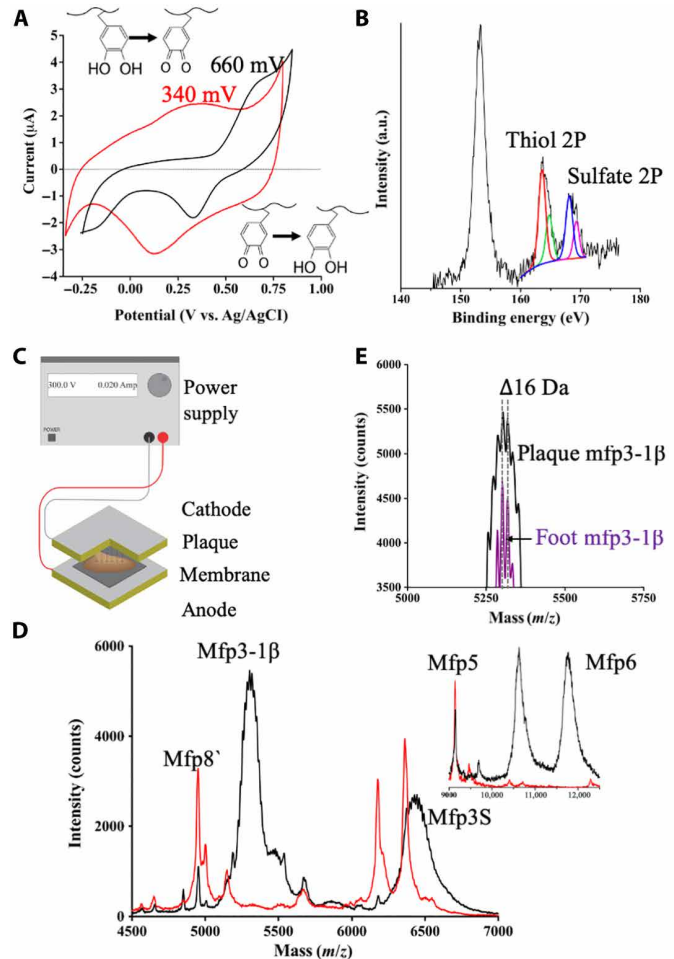
may adaptively tune phase boundaries. Mfp5's solubility at both pHs suggests a reversible association with the separated phase.

We deduced unexpected insights about plaque redox from the sawtooth steps around the mfp3-1β variant peak (with m/z 5304 representing 7 Tyr to Dopa conversions) (Fig. 2E). Step m/z registers provide fiducial markers of redox: Each Dopa oxidized to dopaquinone reduces the mass by 2 Da, or 20 Da for every 10 dopaquinones. Loss of another 2 Da/Dopa or 40 Da/10 Dopas occurs upon quinone tautomer (dehydroDopa) oxidation (*26*). Thus, in the absence of intermolecular adduct formation, oxidation results in a decreasing centroid m/z. As both 24-hour-old plaque and purified mfp3-1β share the same centroid and step masses, oxidation is absent. After 14 days in seawater, however, the centroid m/z for plaque mfp3-1β decreased by ~7 Da. In contrast, the centroid for mfp3S decreased by ~20 Da (fig. S3, A and C), suggesting that variant mfps have differential susceptibilities to oxidation.

Recoacervation of plaque proteins

Detecting pH-dependent phase changes in plaques falls short of detecting dynamic liquid phases in situ, so we focused on LLPS reconstitution of plaque-extracted proteins. Our coacervation of plaque proteins with sulfate (30 mM) corroborated reports of sulfate-mediated coacervation of recombinant mfp3F (9, 10) and was visualized by intrinsic mfp3 fluorescence (Fig. 3A) (15). In minutes, droplet dispersions settled and spread over surfaces (fig. 3AB). Sedimented droplets exhibited the same pattern of saw-toothed mfp3 and mfp6 peaks to within 1 Da of fiducial m/z markers but contained no detectable mfp5 or mfp8 (fig. S3A). We were initially concerned that protein mass spectrometry and acid-urea gel electrophoresis did not appear to agree with respect to mfp3-1β presence in sulfate-induced coacervates. This was resolved by blotting the mfp3S gel band to nitrocellulose and showing by mass spectrometry that the band contained both mfp3S and mfp3-1β variants, i.e., evidence of a strong interaction (fig. S2, D and E). Notably, mfp3S variants (m/z ~6200) coacervated in vitro showed evidence of oxidation after one coacervation/solubilization cycle (fig. S3), corroborating differential variant susceptibility. Inhomogeneous droplet compositions are suggested by coacervating plaque proteins with Alexa Fluor 555 C_2–labeled mfp6 (fig. S4).
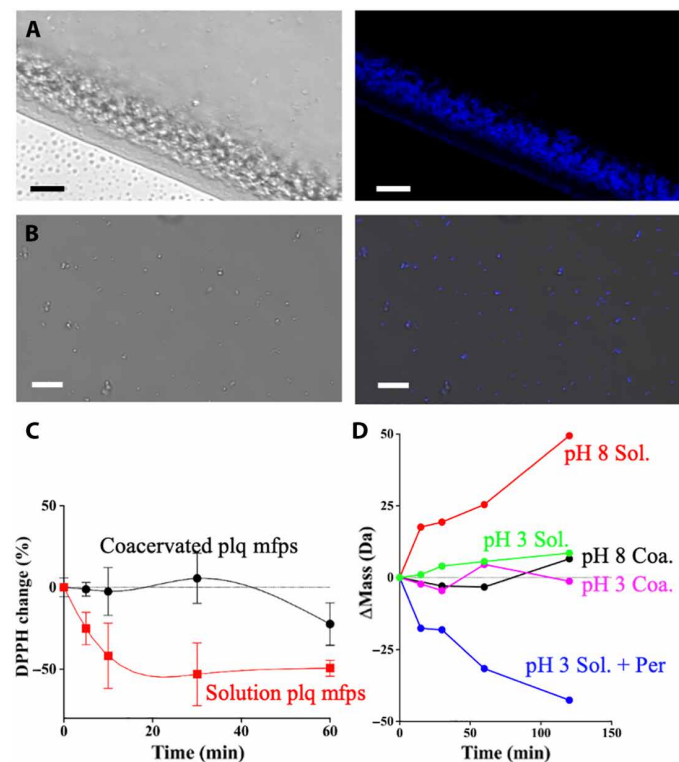
Proteins bulk-extracted from plaques at pH 3 exhibited an anodic peak potential (E_a) of +440 mV with a linear plot of current versus scan rate$^{1/2}$, indicating soluble mfps with reversible DOPA redox (figs. S5 and S1B). When the same cohort of mfps was coacervated by sulfate, Dopa E_a was +101 mV more resistant to oxidation, but redox was less reversible (fig. S5, A and E).

Phase-dependent redox shielding

To confirm redox insulation, we compared redox exchange by soluble and coacervated mfps with two strong oxidants, the redox dye diphenylpicrylhydrazyl radical (DPPH·; E_0' + 0.6 V versus Ag/AgCl) (21) and periodate (E_0' + 1.2 V). Exchange between DPPH· and soluble plaque–derived mfps at pH 8 was detected by DPPH· bleaching (Fig. 3C); in contrast, sulfate-coacervated mfps resisted redox exchange for ~50 min (Fig. 3C and fig. S3C). Coacervated mfps also resisted redox exchange with periodate such that no change in centroid m/z was observed in coacervated samples at either pH 3 or pH 8 for >120 min (Fig. 3D).

DISCUSSION

Mussel wet adhesion hinges on maintaining redox-regulated compartments of Dopa in the plaque, but there is no insight on how these compartments are maintained outside living cells. The most recent model of mussel adhesive plaque structure depicts a fluid-filled spongy solid (Fig. 4A) with mfp3 and mfp5 as interfacial adhesive primers (14). The model proposes that the spongy architecture arises by phase inversion in a secreted colloidal dispersion in which the new continuous phase, consisting of mfp2 and collagen, becomes a solid porous scaffold following structural arrest. The fluid was never characterized, and important details about the phase inversion remain unknown. Mfp6, a nonadhesive antioxidant, is cosecreted with mfp3 and mfp5 (18), but their phase relationship was never determined. The model proposed that Dopa oxidation is rescued by thiols in mfp6, but not how thiol oxidation per se is prevented.

By focusing on the plaque interface, phases, and redox, our new findings support the model's overall placement of proteins in the plaque but adds an important insight to this picture: mfp5 is a thin adhesive priming film connected to a scaffold that is imbibed with mfp3/mfp6-containing liquid-liquid phase–separated droplets in which Dopa and thiol redox are insulated from the ambient equilibrium conditions. We propose that mfp3 and mfp6 donate electrons and protons to keep mfp5 reduced, but the mechanism of this transfer is yet to be determined.

A new model (Fig. 4B) reconciling specific proteins with different phase-based compartments includes C1 as a 15-nm-thick interfacial film of mfp5 (and perhaps mfp8) with a high E_{an}, and C2 as a 10- to 20-nm open-pore mesh filled with interconnected coacervate droplets of mfp3 and mfp6 and an E_{an} ~120 mV lower than C1. We propose the following redox interplay to maintain Dopa-dependent adhesion (Fig. 4B): (i) Dopa-containing interfacial mfps in C1 regularly sustain damage by oxidation to quinone; (ii) unable to rebind the surface, the C1 quinone H-bonds to accessible Dopa in C2, and, given the notably more positive E_{an} of C1 Dopa, undergoes redox exchange to restore Dopa for adhesion; (iii) C2 Mfp3 now has dopaquinone, which it recycles to catechol using $2e^- + 2H^+$ from two thiols in mfp6, or by simple tautomerization to the vinylcatechol (26). Dopa and thiol groups in C2 thus provide a lifeline of electrons and protons for oxidized Dopa in C1 until the reservoir is depleted.
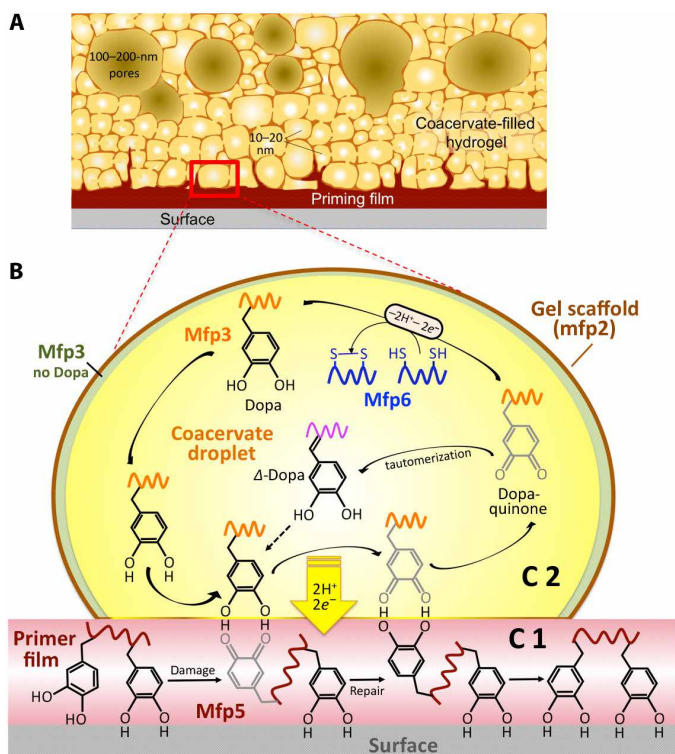

Fig. 3. Behavior of reconstituted plaque coacervates. (**A**) Confocal images of settled (top) and (**B**) suspended (bottom) coacervate (Coa.) protein microdroplets. Visible micrograph (left) and fluorescent image (right). Scale bar: 5 μm. (**C**) Comparing redox exchange between 0.1 mM DPPH and plaque (plq) protein/sulfate coacervates or soluble (Sol.) plaque proteins. Oxidized DPPH is purple (λ_{max}, 515 nm) and undergoes bleaching by reductive redox exchange with available Dopa and/or thiol groups. % change DPPH denotes [DPPH − DPPH$_2$]/DPPH × 100 or the proportion by which initial DPPH color decreases over time. (**D**) Redox exchange between 10 mM periodate (Per) and soluble or coacervated plaque proteins at pH 3 and 8. At pH 8, oxidation occurs without periodate, and quinones add tris to increase in mass.

Fig. 4. Phase-specific Dopa and thiol redox in coacervated plaque proteins. (**A**) Schematic plaque interface. (**B**) Enlarged droplet with mfp3 and mfp6 variants. **C1** is the film below the droplet and contains adhesive primers mfp5 and mfp8. When **C1** Dopa is oxidized to dopaquinone (E_a + 660 mV Ag/AgCl; table S3), the damage is repaired with $2H^+ + 2e^-$ donated by **C2** (E_a + 540 mV). **C2** dopaquinone is reduced back to Dopa by thiols in mfp6 (E_a, −200 mV), but when thiols are depleted, Dopa derivatives (Δ-Dopa) provide reducing poise. Bidentate hydroquinone-quinone interactions actuate redox exchange in many cellular pathways (*29*).

Our results reveal that mussel plaques are core-shell structures with the adhesive film and plaque cuticle as the shell and a coacervate-filled hydrogel as the core. Although hydrogels are receiving much scrutiny for engineering tough interfaces (*27*), replacement of the water with coacervates in these gels is a novel twist that merits particular scrutiny. Coacervation as a natural strategy for protecting redox-sensitive functionalities from oxidation has a profound bearing on improved translation of wet adhesion (*28, 29*) and phase-specific redox in phase-separated compartments elsewhere in biology (*1, 30*). Evidently, by sequestering oxidation prone groups within fluid-filled inclusions in a porous structure like the plaque, the groups can be shielded and recruited for redox exchange with external functionalities damaged by oxidation.

MATERIALS AND METHODS
Plaque collections
California mussels *M. californianus* Conrad harvested from Goleta Pier (34.414088, −119.828690) were held in tanks with circulating natural seawater at 12° to 16°C. To prepare the intact mussel plaques for analysis (Fig. 1B), the mussels were tethered over target substrates such as mica coated with nanometer-thick gold films, mica, glass slides, or, for easy sectioning, Saran wrap. In the case of gold-plated mica, the gold layer remained firmly attached to the plaque but was easily detached from mica surface by gentle tension on the plaque. This approach keeps intact the interfacial plaque chemistry and structure.

Transmission electron microscopy of phase transitions
All plaques intended for transmission electron microscopy (TEM) were collected from the same individual and deposited onto Saran wrap. Half were processed directly for electron microscopy after optimizing the fixation conditions. Half were placed in 5% acetic acid (15°C) for 30 min before processing. All fixation and washing steps were performed on ice. Fresh plaques were fixed in 2% formaldehyde, 2.5% glutaraldehyde, and fixation buffer [200 mM sodium cacodylate, and 300 mM NaCl (pH 7.2)] for 2 hours. The samples were washed three times (10 min each) in degassed fixation buffer and then postfixed in 2% osmium tetroxide in degassed fixation buffer for 2 hours. The samples were then washed four times (10 min each) in degassed deionized water and then dehydrated through a graded series of ethanol washes (25, 50, 75, 90, 100, 100, and 100% ethanol, 10 min each). Solvent was then switched to propylene oxide by washing in 33, 66, 100, 100, and 100% propylene oxide in ethanol. The samples were then infiltrated with epoxy resin (Embed812, Electron Microscopy Sciences, Hatfield, USA), incubating the sample in resin diluted in propylene oxide as follows: 33% (2 hours), 66% (16 hours), and 100% (4 hours). Last, samples were placed in molds and cured at 60°C for 24 hours. Thin sections (60 to 80 nm) for TEM and semithin sections (300 nm) for electron tomography were cut on an EM UC6 ultramicrotome (Leica Biosystems, Wetzlar, Germany). Sections were mounted on copper TEM grids and poststained on drops of uranyl acetate and lead citrate following standard protocols (*31*). All samples were investigated with a Tecnai G2 transmission electron microscope (FEI, Hillsboro, Oregon) operating at 200 kV, and micrographs were recorded with a Gatan Ultrascan charge-coupled device camera (2048 Å, 2048 pixels).

Cyclic voltammetry
CV was performed at room temperature on a Versastat 3 Potentiostat (Ametek Co., Berwyn, PA), with a typical three-electrode cell using Pt wire as the counter electrode, Ag/AgCl as the reference electrode, and gold or glassy carbon (3-mm disc electrodes from BASi, W Lafayette, IN) as the working electrode at 22°C and 1-atm pressure. To avoid interference by adsorbed chemicals on the surface of the working electrode, the following cleaning method was applied to gold electrodes before each experiment: (i) mechanical polishing of the electrode was done using a diamond particle abrasion solution of 1-, 0.25-, and 0.05-μm particle sizes (Buehler, Lake Bluff, IL) for 2 min each on a nylon disk. The electrode was rinsed with water and sonicated for 2 min in a shallow vessel containing water to remove excess diamond particles. (ii) The electrode was then stripped by repetitive cycling between −400 and +1400 mV (versus Ag/AgCl) at a rate of 100 mV/s in 50 mM sulfuric acid until the CV became stable (typically 12 cycles). For abrasive polishing of glassy carbon electrodes, diamond particles were replaced with alumina particles of equivalent size. Analyte autoxidation was minimized by performing all electrochemical experiments with degassed deionized water in a glove bag under argon. Some CV measurements required notable adaptations: For detached plaques, for example, we used dialysis membranes (Spectrapor MWCO 1000, New Brunswick, NJ) with two O-rings to affix the plaque interface against the working electrode. For reconstituted coacervates, the reference electrode was enclosed in a sleeve of dialysis tubing. Without it, adsorbed coacervates caused notable drift.

Electrotransfer of plaque proteins

To capture proteins undergoing a phase change from a condensed state to solution, plaques naturally deposited by mussels onto glass slides (Fisher Scientific 12-544-7) were collected by severing the connecting distal thread within 24 hours of deposition. While attached to the slide, each plaque was rinsed for 60 s with 18-megohm pure water (MilliPore, Burlington, MA). Following rinsing, plaques were incubated in either 5% acetic acid or filtered seawater for 30 min at room temperature, with shaking at 45 rpm. Seawater-treated plaques required additional washing step after treatment to remove excess salts, which interfere with the electrophoretic process. These plaques were washed three times per minute each with transfer buffer. Following incubation, plaques were peeled from the slide with a clean single-edge razor blade. Excised plaques were placed between two 0.45-μm nitrocellulose membranes (NitroPure WP4HY08250, Life Science Products, Frederick, CO) and loaded into a semidry transfer cell (Bio-Rad Trans-Blot SD no. 1703940, Hercules, CA). The 5% acetic acid–conditioned plaques were electrophoresed in 0.7% acetic acid at 12 V for 20 min. The seawater-conditioned plaques were electrophoresed in 121 mM tris-glycinate (pH 8.2) at 12 V for 20 min. Although the direction of electrophoresis was initially performed in both directions, soluble components migrated only toward the cathode. As a result, the plaque-substrate interface must face the cathode during acidic transfers and the anode during basic transfers.

Mass spectrometry

Proteins transferred to nitrocellulose membranes were investigated in situ by matrix-assisted laser desorption/ionization–time-of-flight (MALDI-TOF) mass spectrometry. For postelectroblotting transfer, the membrane was cut around the perimeter of the plaque footprint using a clean no. 11 scalpel. With fine-nose tweezers, the plaque was removed from the membrane, which is subsequently affixed to a MSP 96 MALDI Target (Bruker, Billerica, MA) with adhesive carbon tape. Ten microliters of MALDI matrix, a saturated solution of α-cyano-4-hydroxycinnamic acid in 30% acetonitrile 1% trifluoroacetic acid, was applied to the membrane and dried in a vacuum desiccator (Nalgene). Mass spectrometry analysis was conducted using a Microflex LRF MALDI-TOF (Bruker, Billerica, MA). Sample membranes were irradiated using a nitrogen laser at 337 nm and a pulse length of 3 ns with a repetition rate of 20 Hz. Detection occurred in a linear mode between 2 and 20 kDa at a sampling rate of 1 Gs/s. Protein Calibration Standard 1 (Bruker no. 206355) was used as an internal calibration.

Oxidative damage to proteins was assessed by mass spectrometry. Plaques less than 48 hours old were homogenized in 10 mM acetic acid at a ratio of ~50-mg wet weight to 1 ml of acetic acid using a Dounce homogenizer. The homogenate was clarified via centrifugation at 5000g for 5 min after which the soluble supernatant was carefully separated from the insoluble fraction. The concentration of protein was assessed via the Bradford assay kit (Thermo Fisher Pierce, Waltham, MA) and adjusted to 1 mg/ml with 10 mM acetic acid. The solution was aliquoted into five samples and adjusted to assay conditions using the following stock buffers: (i) 10 mM acetic acid, (ii) 10 mM acetic acid + 10 mM sodium metaperiodate (Sigma-Aldrich), (iii) 50 mM tris (pH 8.0), (iv) 50 mM tris (pH 8.0; coacervate), and (v) 10 mM acetic acid (coacervate) + 10 mM sodium metaperiodate.

Oxidation was tracked by acquiring spectra as time elapsed. The sample was mixed with α-cyano-4-hydroxycinnamic acid in 50% (v/v) aqueous acetonitrile with 0.1% trifluoroacetic acid at a ratio 1:9 and spotted onto a stainless steel MALDI target.

Amino acid analysis of electrotransferred footprints

Electrotransfer was performed as above, except that NitroPure membranes were replaced with polyvinylidene difluoride membranes (Immobilon IPVH00005). This change avoided nitrocellulose degradation in 6 N HCl. Five blotted footprints were excised from the excess membrane and loaded into a 1-ml glass ampule (Wheaton Glass, no. 651502, Millville, NJ) and submerged with 250 μl of constant boiling 6 N HCl with 10 μl of phenol. Acid hydrolysis of electrotransferred proteins was done at 110°C for 24 hours under vacuum. After 24 hours, the sample was removed from the vial and loaded into a LoBind microcentrifuge tube (Eppendorf, no. Z666505). The hydrolysis ampule was washed with 500-μl X2 of 18-megohm pure water to ensure that all amino acids were transferred to the microcentrifuge tube. The now dilute HCl was removed via flash evaporation with a SpeedVac vacuum concentrator with vapor trap (Savant, Holbrook, NY). Once dried, amino acids were resuspended in 200 μl of 0.01 N HCl and loaded into the automated amino acid analyzer (Hitachi High-Technologies model L-8900, Ibaraki, Japan).

Polyacrylamide gel electrophoresis of plaque extracts

Proteins can be electrokinetically extracted from single plaques for microanalysis by mass spectrometry and amino acid analysis, but these quantities are insufficient to see on a gel or to coacervate. For gels, plaques (<24 hours old) were collected and pooled for bulk homogenization at a ratio of ~50-mg wet weight to 1 ml of either 0.7% acetic acid (pH 3) or 121 mM tris-glycinate (pH 8.2) to match electrotransfer conditions. The homogenate was clarified via centrifugation at 5000g for 10 min at which point the supernatant solution was carefully separated from the insoluble fraction. The pH 8.2 homogenate was then dialyzed against 0.7% acetic acid for >4 hours at 4°C. Both homogenates were mixed 1:1 with gel-loading buffer (5% acetic acid and 8 M urea) (*32*), and 10 μl was loaded onto a preequilibrated 7.5% acid-urea gel (10 mA for 2 hours). The gel was run with 5% acetic acid, serving as the tank buffer in a Bio-Rad Mini-PROTEAN Tetra Cell (Hercules, CA) at a constant current of 12 mA for 30 min using a GE EPS 301 power supply. After electrophoresis, the gel was stained with 0.1% Coomassie Brilliant Blue (CBB) G-250 in 40% methanol and 20% acetic acid for 30 min and destained with 20% methanol and 10% acetic acid until the gel background became completely transparent.

Mass spectrometry analysis of polyacrylamide gel electrophoresis bands

Acid-urea–polyacrylamide gel electrophoresis (PAGE) experiments were conducted, as stated above. Before electrophoretic transfer, extra thick blotting paper, nitrocellulose membranes, and PAGE gel were equilibrated in 0.7% acetic acid for 10 min. PAGE gels were placed between two 0.45-μm nitrocellulose membranes (NitroPure WP4HY08250) and loaded into a semidry transfer cell (BioRad Transblot SD no. 1703940). The 5% acetic acid–conditioned plaques were electrophoresed in 0.7% acetic acid at 13 V for 15 min. Duplicate lanes of each sample were run and the membrane cut in half, so that one lane could be visualized via Coomassie staining and one lane could be excised from the membrane for mass spectrometry

analysis. The excised membrane is subsequently affixed to a MSP 96 MALDI Target (Bruker) with adhesive carbon tape. Ten microliters of MALDI matrix, a saturated solution of α-cyano-4-hydroxycinnamic acid in 30% acetonitrile and 1% trifluoroacetic acid, was applied to the membrane and dried in a vacuum desiccator (Nalgene). Mass spectrometry analysis was conducted using a Microflex LRF MALDI-TOF (Bruker). Sample membranes were irradiated using a nitrogen laser at 337 nm and a pulse length of 3 ns with a repetition rate of 20 Hz. Detection occurred in a linear mode between 2 and 20 kDa at a sampling rate of 1 Gs/s. Protein Calibration Standard 1 (Bruker no. 206355) was used as an internal calibration.

Analyses of bulk extracted plaque proteins
Thiol and Dopa quantification
Because Dopa and cysteine are important to protein redox, these functionalities were independently quantified for comparison to amino acid analysis. Plaques (<48 hours old) were homogenized in 10 mM acetic acid at a ratio of ~50-mg wet weight to 1 ml of acetic acid using a Dounce homogenizer on ice. The homogenate was clarified via centrifugation at 5000g for 10 min, effectively separating the soluble supernatant from the insoluble pellet. A stock of Ellman's Reagent (Thermo Fisher Scientific, Waltham, MA) was made 4 mg/ml in dimethyl sulfoxide. Guanidine-HCl (Fisher) was dissolved in reaction buffer [RB; 0.1 M Hepes and 1 mM EDTA (pH 8)] to a final concentration of 6 M. RB (107 µl) was added to 30 µl of guanidine and 40 µl of homogenate and mixed via aspiration to ensure homogeneity of the solution. Ten microliters of stock Ellman's Reagent was added to the mixture and allowed to react for 15 min before measuring the absorbance at 412 nm (33). Concentration of thiols in the homogenate was calculated from a standard curve of cysteine-HCl monohydrate. The standard curve was created by make twofold serial dilutions of cysteine from 2 to 0.08 mM. Dopa was quantified in aliquots of the 10 mM extract supernatants using an adaptation of the Arnow assay (34) with L-Dopa or 4-methyl catechol as calibration standards.

Plaque sulfate
Sulfate-mediated coacervation is not biologically relevant to mfps in plaques, unless sulfate levels are elevated at the plaque interface. A two-component 5-min epoxy was mixed and deposited into a 6 mm by 6 mm square face mold (Electron Microscopy Sciences, Hatfield, PA). A fresh mussel plaque was excised from the mussel using a clean single-edge razor and mounted with the thread down (plaque interface up) into the exposed underside of partially cured epoxy. Sulfate was detected via x-ray photoelectron spectroscopy using a Thermo Fisher Scientific ESCALAB XI spectrometer with Al Kα x-ray source. An overview spectrum was gathered from 700 to 0 eV with a 0.5-eV step size and 100-ms dwell time. A high-resolution spectrum of the sulfur K-edge was then collected from 175 to 144 eV with a 0.1-eV step size and 250-ms dwell time and summed over six scans. Sulfate was identified using the Casa software (Teignmouth, UK), fitting the S 2p$^{3/2}$ with a Gaussian function centered at 168.12 eV, with a full width height mean of 1.35 eV separated from 2p$^{1/2}$ by 1.18 eV (169.3 eV) constrained to an intensity ratio of 2:1.

Redox assays using DPPH·
DPPH (redox potential = +0.77 V standard hydrogen electrode; see table S3) is a redox dye that can be used to quantify a wide variety of reducing compounds with lower redox potentials. Plaques (<48 hours old) were collected and homogenized in 10 mM acetic acid at ~50-mg wet weight per 1 ml of acetic acid, using a Dounce homogenizer.

The homogenate was clarified via sedimentation at 5000g for 5 min after which the soluble supernatant was carefully decanted from the insoluble fraction. The concentration of protein was determined by the Bradford assay and adjusted to 1 mg/ml. The redox capacity of the solution was assessed using a published DPPH assay protocol (35). Fifty microliters of protein solution was added to 900 µl of assay buffer [100 mM Hepes (pH 7.4)]. For coacervate assays, an aliquot of 1 M Na$_2$SO$_4$ stock was added to a final concentration of 30 mM to solutions containing soluble protein (1 mg/ml) and mixed with assay buffer by rapid in-out pipetting. To begin the redox reaction, 50 µl of 2 mM stock DPPH (Sigma-Aldrich, St Louis, MO) solution (in methanol) was added to the protein-containing solution. The absorbance at 517 nm was monitored as a function of time. The percentage of oxidized DPPH reagent remaining as a function of time was calculated as % DPPH remaining = (Abs$_{\text{sample},t}$/Abs$_{\text{control},t}$ × 100).

Reconstituted coacervation and labeling of plaque proteins
Coacervation requires milligram amounts of protein, particularly for doing coacervate electrochemistry and redox assays with DPPH. In vitro coacervation of plaque protein extracts was affected by sulfate addition, which Bungenberg de Jonge (36) referred to as "complex coacervation" between microanions and macrocations. Notably, two groups have investigated on the phase behavior of recombinant mfp3 variants coacervated by microanions such as sulfate, phosphate, and citrate (9, 10). At a protein concentration of 1 mg/ml, both reported a coacervate phase boundary at 20 to 40 mM sulfate, which approximates the sulfate concentration in seawater. One hundred–milligram wet weight of plaques were collected and rinsed three times for 1 min with deionized water and then one time with marine phosphate-buffered saline (mPBS). Plaques were homogenized in 10 mM acetic acid at a ratio of 100 mg/1 ml. The homogenate was clarified via centrifugation at 5000g for 10 min. The resulting clarified homogenate was filtered with a 0.22-µm filter and adjusted to protein (1 mg/ml) with 10 mM acetic acid as necessary. Coacervation was induced by adding stock 1 M sodium sulfate to a final concentration of 30 mM. Confocal images of phase separation were collected using a Leica SP8 confocal microscope (Leica Microsystems, Wetzlar, Germany) fitted with 63×/1.4–numerical aperture oil immersion objective and hybrid detectors (HyD). Coacervates were visualized via the intrinsic fluorescence of mfp3 excited with a 405-nm laser (7). In a parallel experiment in coacervating mfps in which two distinct fluorophores are present, rinsed plaques were then incubated in 0.05 µM Alexa Fluor 555 C$_2$ maleimide (Thermo Fisher Scientific, Waltham, MA) in mPBS at room temperature for 2 hours while rotating on a mixer. Alexa Fluor 555 C$_2$ maleimide specifically targets Cys residues, which are limited to mfp6. Following incubation, plaques were rinsed three times for 1 min with 10 ml of deionized water to remove excess fluorophore. Alexa Fluor 555–stained coacervates were visualized using the white light laser tuned to 550-nm excitation.

SUPPLEMENTARY MATERIALS

REFERENCES AND NOTES
1. A. A. Hyman, C. A. Weber, F. Jülicher, Liquid-liquid phase separation in biology. *Annu. Rev. Cell Dev. Biol.* **30**, 39–58 (2014).
2. B. Vrhovski, S. Jensen, A. S. Weiss, Coacervation characteristics of recombinant human tropoelastin. *FEBS Journal* **250**, 92–98 (1997).

3. H.-J. Jin, D. L. Kaplan, Mechanism of silk processing in insects and spiders. *Nature* **424**, 1057–1061 (2003).

4. Y. P. Tan, S. Hoon, P. A. Guerette, W. Wei, A. Ghadban, C. Hao, A. Miserez, J. H. Waite, Infiltration of a chitin by protein coacervates defines the squid beak mechanical gradient. *Nat. Chem. Biol.* **11**, 489–495 (2015).

5. M. Yamanaka, Y. Ishizaki, T. Nagakawa, A. Taoka, Y. Fukumori, Purification and characterization of coacervate-forming cuticular proteins from *Papilio xuthus* pupae. *Zoolog. Sci.* **30**, 534–542 (2013).

6. H. Zhao, C. J. Sun, R. J. Stewart, J. H. Waite, Cement proteins of the tube building polychaete *Phragmatopoma californica*. *J. Biol. Chem.* **280**, 42938–42944 (2005).

7. W. Wei, Y. Tan, N. R. Martinez Rodriguez, J. Yu, J. N. Israelachvili, J. H. Waite, A mussel-derived one-component adhesive coacervate. *Acta Biomater.* **10**, 1663–1670 (2013).

8. D. G. DeMartini, J. M. Errico, S. Sjöström, A. Fenster, J. H. Waite, A cohort of new adhesive proteins identified from transcriptomic analysis of mussel foot glands. *J. R. Soc. Interface* **14**, 20170151 (2017).

9. B. Yang, S. Jin, Y. Park, Y. M. Jung, H. J. Cha, Coacervation of interfacial adhesive proteins for initial adhesion to a wet surface. *Small* **14**, e1803377 (2018).

10. J. Wang, T. Scheibel, Coacervation of the recombinant *Mytilus galloprovincialis* foot protein-3b. *Biomacromolecules* **19**, 3612–3619 (2018).

11. S. Kim, H. Y. Yoo, J. Huang, Y. Lee, S. Park, S. Park, S. Jin, Y. M. Jung, H. Zeng, D. S. Hwang, Y. Jho, Salt triggers the simple coacervation of an underwater adhesive when cations meet aromatic π electrons in seawater. *ACS Nano* **11**, 6764–6772 (2017).

12. D. S. Hwang, H. Zeng, A. Srivastava, D. V. Krogstad, M. Tirrell, J. N. Israelachvili, J. H. Waite, Viscosity and interfacial properties in a mussel-inspired adhesive coacervate. *Soft Matter* **6**, 3232–3236 (2010).

13. I. Kaminker, W. Wei, A. M. Schrader, Y. Talmon, M. T. Valentine, J. N. Israelachvili, J. H. Waite, S. Han, Simple peptide coacervates adapted for rapid pressure sensitive wet adhesion. *Soft Matter* **13**, 9122–9131 (2017).

14. J. H. Waite, Mussel adhesion – essential footwork. *J. Exp. Biol.* **220**, 517–530 (2017).

15. J. Saiz-Poseu, J. Mancebo-Aracil, F. Nador, F. Busque, D. Ruiz-Molina, The chemistry behind catechol-based adhesion. *Angew. Chem. Int. Ed.* **58**, 696–714 (2019).

16. G. P. Maier, C. M. Bernt, A. Butler, Catechol oxidation: Considerations in the design of wet adhesive materials. *Biomater. Sci.* **6**, 332–339 (2017).

17. N. R. Martinez Rodriguez, S. Das, Y. Kaufman, J. N. Israelachvili, J. H. Waite, Interfacial pH during mussel adhesive plaque formation. *Biofouling* **31**, 221–227 (2015).

18. J. Yu, W. Wei, E. Danner, R. K. Ashley, J. N. Israelachvili, J. H. Waite, Mussel protein adhesion depends on interprotein thiol-mediated redox modulation. *Nat. Chem. Biol.* **7**, 588–590 (2011).

19. C. Zhong, T. Gurry, A. A. Cheng, J. Downey, Z. Deng, C. M. Stultz, T. K. Lu, Strong underwater adhesives made by self-assembling multiprotein nanofibres. *Nat. Nanotechnol.* **9**, 858–866 (2014).

20. L. H. N. Cooper, Oxidation-reduction potential in sea water. *J. Mar. Biol. Ass. UK* **22**, 167–176 (1937).

21. D. R. Miller, J. E. Spahn, J. H. Waite, The staying power of adhesion-associated antioxidant activity in *Mytilus californianus*. *J. R. Soc. Interface* **12**, 20150614 (2015).

22. A. Jain, R. D. Vale, RNA Phase transitions in repeat expansion disorders. *Nature* **546**, 243–247 (2017).

23. E. Filippidi, D. G. DeMartini, P. Malo de Molina, E. W. Danner, J. Kim, M. E. Helgeson, J. H. Waite, M. T. Valentine, The microscopic network structure of mussel (*Mytilus*) adhesive plaques. *J. R. Soc. Interface* **12**, 20150827 (2015).

24. G. M. Proudfoot, I. M. Ritchie, Cyclic voltammetric study of some 4-substituted benzene-1, 2 diols. *Austral. J. Chem.* **36**, 885–894 (1983).

25. W. Wei, J. Yu, C. C. Broomell, J. N. Israelachvili, J. H. Waite, Hydrophobic enhancement of Dopa mediated adhesion in a mussel foot protein. *J. Am. Chem. Soc.* **135**, 377–383 (2013).

26. R. Mirshafian, W. Wei, J. N. Israelachvili, J. H. Waite, α, β-dehydro-Dopa: A hidden participant in mussel adhesion. *Biochemistry* **55**, 743–750 (2016).

27. J. Yang, R. Bai, B. Chen, Z. Suo, Hydrogel adhesion: A supramolecular synergy of chemistry, topology, and mechanics. *Adv. Func. Mat.* **30**, 1901693 (2019).

28. J. Heo, T. Kang, S. G. Jang, D. S. Hwang, J. M. Spruell, K. L. Killops, J. H. Waite, C. J. Hawker, Improved performance of protected catecholic polysiloxanes for bioinspired wet adhesion to surface oxides. *J. Am. Chem. Soc.* **134**, 20134–20145 (2012).

29. Q. Zhao, D. W. Lee, B. K. Ahn, S. Seo, Y. Kaufman, J. N. Israelachvili, J. H. Waite, Underwater contact adhesion and microarchitecture in polyelectrolyte complexes actuated by solvent exchange. *Nat. Mater.* **15**, 407–412 (2016).

30. Y. Shin, C. P. Brangwynne, Liquid phase condensation in cell physiology and disease. *Science* **357**, eaaf4382 (2017).

31. C. A. Monnier, D. G. DeMartini, J. H. Waite, Intertidal exposure favors soft-studded armors of adaptive mussel coatings. *Nat. Commun.* **9**, 3424 (2018).

32. S. Panyim, R. Chalkley, High resolution acrylamide gel electrophoresis of histones. *Arch. Biochem. Biophys.* **130**, 337–346 (1969).

33. T. E. Creighton, in *Protein Structure – A Practical Approach* (IRL Press, 1989), pp. 155–168.

34. J. H. Waite, M. L. Tanzer, Specific colorimetric detection of *o*-diphenols and 3,4-dihydroxycontaining peptides. *Anal. Biochem.* **111**, 131–136 (1981).

35. S. C. T. Nicklisch, J. E. Spahn, H. Zhou, C. M. Gruian, J. H. Waite, Redox capacity of an extracellular matrix protein associated with adhesion in *Mytilus californianus*. *Biochemistry* **55**, 2022–2030 (2016).

36. H. G. Bungenberg de Jonge, Complex colloid systems, in *Colloid Science*, H. R. Kruyt, Ed. (Elsevier, 1949), pp. 335–400.

37. H. Zhao, J. H. Waite, Linking adhesive and structural proteins in the attachment plaque of *Mytilus californianus*. *J. Biol. Chem.* **281**, 26150–26158 (2006).

38. H. Zhao, N. B. Robertson, S. A. Jewhurst, J. H. Waite, Probing the adhesive footprints of *Mytilus californianus* byssus. *J. Biol. Chem.* **281**, 11090–11096 (2006).

Citation: E. Valois, R. Mirshafian, J. H. Waite, Phase-dependent redox insulation in mussel adhesion. *Sci. Adv.* **6**, eaaz6486 (2020).